DE GRUYTER OPEN
Studia Geotechnica et Mechanica, Vol. 37, No. 2, 2015
DOI: 10.1515/sgem-2015-0022

IMPROVED FORMULATION OF THE HARDENING SOIL MODEL IN THE CONTEXT OF MODELING THE UNDRAINED BEHAVIOR OF COHESIVE SOILS

ANDRZEJ TRUTY

Institute of Geotechnics, Cracow University of Technology, Poland

RAFAŁ OBRZUD

GeoMod S.A., Switzerland

Abstract: The analysis of an important drawback of the well known Hardening Soil model (HSM) is the main purpose of this paper. A special emphasis is put on modifying the HSM to enable an appropriate prediction of the undrained shear strength using a non-zero dilatancy angle. In this light, the paper demonstrates an advanced numerical finite element modeling addressed to practical geotechnical problems. The main focus is put on serviceability limit state analysis of a twin-tunnel excavation in London clay. The two-phase formulation for partially saturated medium, after Aubry and Ozanam, is used to describe interaction between soil skeleton and pore water pressure.

Key words: *soil constitutive modeling, undrained shear strength, deep excavations*

1. INTRODUCTION

An analysis of static or dynamic soil-structure interaction problem with reference to serviceability limit states, in particular, is one of the most challenging tasks in the modern geotechnical engineering. Some of them, like deep excavations or foundation rafts stiffened by piles or displacement columns, require applying advanced numerical modeling tools which are based on the finite element, finite difference or a wide class of meshless methods. The two most important features, i.e., availability of robust constitutive laws to describe soil behavior with a special emphasis on the strong stiffness variation in the range of small strains and two-phase formulations including an extension to partially-saturated media seem to be crucial to tackle the aforementioned class of problems. For many years geotechnical community was in strong opposition to this methodology showing that advanced numerical modeling may yield poor or very poor predictions for complex practical problems. The main goal of this paper is to demonstrate that advanced numerical modeling with the aid of the Hardening Soil (HS) model with an extension to the small strain stiffness (HSs) describing a complex soil behaviour, can be a robust tool in hands of a practicing engineer.

This paper is organized as follows. A short reminder of the simplified formulation for a two-phase partially saturated medium, by Aubry and Ozanam [3], is given in Section 2. In the next section, important drawbacks related to ability of reproducing undrained behavior of cohesive soils by the original version of HS model are discussed and possible remedies are proposed. The next section shows a number of undrained triaxial compression test simulations carried out on normally- and overconsolidated material which are analyzed in the light of the modified formulation of the HS model. Finally, Section 5 illustrates a case study of a tunnel excavation in London clay. The last section provides conclusions and final remarks.

2. MAJOR ASPECTS OF TWO-PHASE FORMULATION FOR PARTIALLY SATURATED MEDIA

An appropriate modeling of soil-structure interaction problems using any advanced constitutive model

for soil, and relying on effective stress parameters, requires considering a coupled analysis of deformation and pore water fluid flow. In most cases, a part of the analyzed domain remains in partially saturated zone in which suction pressure exists and generates an apparent cohesion effect. The zone below a free ground water table is typically considered as fully saturated. Therefore, the time scale effect may play an important role when analyzing typical geotechnical problems such as deep excavations, retaining walls, especially in poorly permeable deposits.

In ZSoil, a finite element code, a consistent two-phase formulation of partially saturated medium is used following the theory proposed by Aubry and Ozanam [3]. Due to a limited scope of this paper, we focus our attention only on the most important aspects of this formulation, limited here to the static cases.

In this theory, the overall equilibrium equation for the solid and fluid phases is written in the following form

$$\sigma_{ij,j}^{\mathrm{tot}} + \rho g b_i = 0, \tag{1}$$

$$\rho = \rho_{\mathrm{dry}} + nS\rho^{\mathrm{F}}, \tag{2}$$

with total stress components denoted by $\sigma_{ij}^{\mathrm{tot}}$, gravity g, solid skeleton bulk density ρ_{dry}, water specific weight γ^{F}, porosity n and current saturation ratio by S. The total stress obeys the effective stress principle after Bishop

$$\sigma_{ij}^{\mathrm{tot}} = \sigma_{ij} + \delta_{ij} S p \tag{3}$$

with δ_{ij} denoting Kronecker's symbol, σ_{ij} effective stresses, and p is the pore pressure.

The fluid flow continuity equation including the effect of compressibility of the fluid and partial saturation is expressed by the following equation

$$S\dot{\varepsilon}_{kk} + v_{k,k}^{\mathrm{F}} = \left(n\frac{S}{K^{F}} + n\frac{\partial S}{\partial p} \right)\dot{p} \tag{4}$$

with Darcy's velocity vector components denoted by $v_k^{\mathrm{F}} v^{\mathrm{F}}$ and fluid bulk modulus by K^{F}.

The extended Darcy's law which accounts for seepage in the partially saturated zone (gas particles move with the same velocity as fluid ones)

$$v_i^{\mathrm{F}} = k_{ij} k_r(S)\left(\frac{1}{\gamma^{\mathrm{F}}} p_{,j} + b_j \right). \tag{5}$$

The additional equations expressing relations $S(p)$ (a simplified van Genuchten's law [13] to model the soil water retention curve) and $k_r(S)$ (after Irmay [6]) are expressed as follows

$$S = S(p) = \begin{Bmatrix} S_r + \dfrac{1 - S_r}{\left[1 + \left(\alpha \dfrac{p}{\gamma^{\mathrm{F}}} \right)^2 \right]^{1/2}} & \text{if } p < 0 \\ 1 & \text{if } p \geq 0 \end{Bmatrix}, \tag{6}$$

$$k_r(S) = \left(\frac{S - S_r}{1 - S_r} \right)^3, \tag{7}$$

where the residual saturation ratio is denoted by S_r, and a is a material constant which controls the rate of wetting or drying of a partially saturated medium. In other words, $1/\alpha$ defines the height of partially saturated zone.

The balance equations (1) and (4) written here in the strong form, can easily be converted to the weak one, and discretized by means of the standard Galerkin's procedure [11]. Further details concerning this issue and comprehensive explanation of advanced stabilization techniques that are needed to handle quasi-undrained cases can be found in [11], [12].

It is worth noting that suction pressures may generate a strong apparent cohesion effect. Considering Bishop's effective stress principle and van Genuchten's model, we can try to find a limit for the expression $S{\cdot}p$. For $S_r = 0.0$ and $p \to -\infty$ this expression tends to the limit $S \cdot \to -\gamma^{\mathrm{F}}$ a while for $S_r > 0$ such a limit does not exist anymore. This fact must carefully be treated in practical applications.

3. HARDENING SOIL MODEL

The initial version of the Hardening Soil model, including single plastic mechanism with a non-associated flow rule and shear hardening, was first proposed by Schanz [9]. Then the model was modified, by introducing a cap yield surface, by Schanz, Vermeer and Bonnier [10]. The final form of the model including small strain stiffness extension was worked out by Benz [4].

Implementation of HS model in the ZSoil code [1], [8] allowed the first author to propose some improvements, with respect to Benz's version, in order to simplify the numerical stress-strain integration scheme and enhance its robustness. The modifications were mostly related to the definition of the dilatancy law in the contractant domain (in this domain, the value of the mobilized friction angle ϕ_m is smaller than the

critical state friction one ϕ_{cs}) and description of the smooth (in the deviatoric plane) cap yield surface [8].

This model has got a lot of attention of geotechnical engineers in the past few years, as it is able to predict well the deformation and stress states when analyzing the boundary problems such as deep excavations and large foundation rafts (with or without piles).

Although the macroscopic behavior of cohesionless soils can be reproduced by the model reasonably well, regardless of drainage conditions, the ability to represent undrained behavior of overconsolidated, therefore usually dilative, cohesive soils becomes limited. The major drawback of the model is such that it is unable to appropriately reproduce the undrained shear strength in the case when dilatancy angle ψ is larger than zero.

By applying a conservative assumption $\psi = 0°$, the computed undrained shear strength may be underestimated with respect to the true one (even a few times for larger values of OCR). On the other hand, by assuming $\psi > 0°$, the undrained shear strength will tend to infinity with the increasing shear strain amplitude.

In order to explain the source of the aforementioned problem, and to show possible remedies, only important new features of the standard HS model (small strain overlay remains unchanged with respect to Benz's formulation) will be discussed adopting standard soil mechanics notation (compressive stresses are positive).

In the standard HS model hardening laws for the shear and volumetric plastic mechanism are decoupled. The preconsolidation pressure p_c being the hardening parameter of the cap yield surface, depends solely on the accumulated volumetric plastic strain ε_v^c produced by this mechanism. Similar assumption is adopted for the shear yield surface that expands with increasing accumulated deviatoric plastic strain γ^{PS} produced by the shear mechanism. The latter plastic mechanism may also produce volumetric plastic strain (due to dilatancy) but it is not coupled with the hardening law for preconsolidation pressure. If focusing on cohesive soils, the lack of coupling of these two plastic mechanisms leads to an unlimited undrained shear strength increase regardless of the OCR value. In order to better understand this effect, let us consider the undrained triaxial compresion test carried out on normally consolidated sample of a cohesive soil (σ_3' = 1000 kPa) applying a relatively low value of dilatancy angle ψ. The evolution of the effective stress path given by the model is illustrated in Fig. 1. As the sample is normally consolidated the effective stress is represented by a point, in the $p - q$ plane, being an intercept of the current cap and shear yield surfaces (points A, B, for instance). These intersection points play a role of stress attractors from the very beginning of the test. The two specific stages are analyzed in the figure. At point A the stress state is located below zero dilatancy line, while at point B the current shear plastic mechanism is controlled by the Mohr–Coulomb strength envelope, regardless of the value of hardening parameter γ^{PS}. When the point representing the current stress state passes zero dilatancy line, the effective stress path reverses its direction and starts moving upward. As we can notice, the projection measure of the vector normal to the cap yield surface at point B (the associated flow rule is adopted for this mechanism), on the p axis, is always nonzero and positive. In result, compressive plastic volumetric strain is permanently produced by cap mechanism and p_c value may progressively increase. This effect causes an unlimited growth of the cap yield surface caused by dilatancy.

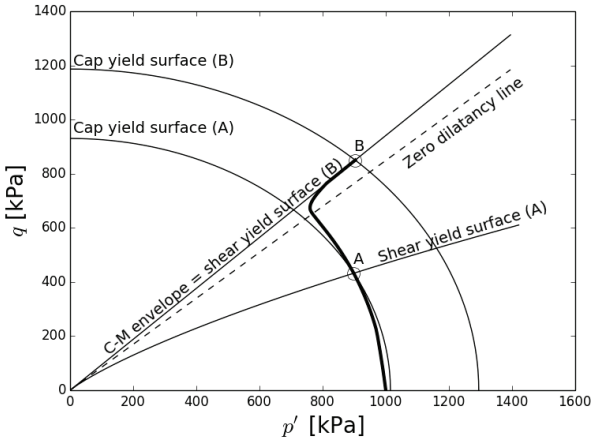

Fig. 1. Evolution of the effective stress path in the undrained triaxial test assuming uncoupled shear/volumetric plastic mechanisms (OCR = 1)

A similar situation will be observed for overconsolidated soil for which effective stress path in the $p - q$ plane will revert its direction at mobilized friction angle being equal to the one at the critical state ($\sin\phi_m = \sin\phi_{cs}$) and then it will follow that line until the current cap yield surface is met. Starting from that moment, the stress state will remain at the point, being the intercept of the two yield surfaces, which will progressively move up.

In order to recover the limit for the ultimate deviatoric shear stress under undrained conditions, both mechanisms have to be coupled by modifying the hardening law for preconsolidation pressure p_c and correcting Rowe's dilatancy law, in the dilatant domain (i.e., $\sin\phi_m > \sin\phi_{cs}$).

A coupled hardening law for the parameter p_c can be expressed as follows

$$\mathrm{d}p_c = H\left(\frac{p_c + c\cot\phi}{\sigma_{\mathrm{ref}} + c\cot\phi}\right)^m (\mathrm{d}\varepsilon_v^{p,c} + \mathrm{d}\varepsilon_v^{p,s}) \qquad (8)$$

where H is a material parameter adjusted from the assumed K_0^{NC} value and the assumed tangent oedometric modulus E_{oed} at a given reference stress, $\mathrm{d}\varepsilon_v^{p,c}$ is the volumetric plastic strain increment caused by the cap mechanism, while $\mathrm{d}\varepsilon_v^{p,s}$ by the shear one.

The modification of Rowe's dilatancy law includes an extra scalar valued function $f_c(x)$ which scales the mobilized dilatancy angle ψ_m with respect to the current value of the overconsolidation ratio OCR.

$$\sin\psi_m = \frac{\sin\phi_m - \sin\phi_{cs}}{1 - \sin\phi_m \sin\phi_{cs}} f_c(x), \qquad (9)$$

$$\sin\phi_m = \frac{\sigma_1 - \sigma_3}{\sigma_1 + \sigma_3 + 2c\cot\phi}, \qquad (10)$$

$$\sin\phi_{cs} = \frac{\sin\phi - \sin\psi}{1 - \sin\phi\sin\psi}. \qquad (11)$$

The newly introduced function $f_c(x)$ is equal to zero for all stress paths satisfying the condition $p > p_{cs}$ and nonzero (varying in the range 0...1) depending on the variable x that is defined according to

$$x = \frac{p + c\cot\phi}{p_{cs} + c\cot\phi}. \qquad (12)$$

The function $f_c(x)$ is defined using the following third order polynomial (3-rd order spline)

$$f_c(x) = 1 - 3x^2 + 2x^3. \qquad (13)$$

It yields zero first order derivatives at $x = 0$ and $x = 1$ while its values at $x = 0$ and $x = 1$ are equal to one and zero, respectively. The p_{cs} value corresponds to the mean effective stress being the intercept of the current shear and volumetric (cap) yield surfaces. For a given stress state σ_{ij} and hardening parameters p_c and γ^{PS}, the value of p_{cs} is defined as follows (see Fig. 2)

$$p_{cs} = \frac{\widetilde{\sigma}_{kk}}{3},$$

$$\widetilde{\sigma}_{kk} = s_{ij}A_1 + \delta_{ij}A_2,$$

$$s_{ij} = \sigma_{ij} - \frac{1}{3}\sigma_{kk}.$$

The two unknowns A_1 and A_2 can easily be obtained by solving the following nonlinear system of two equations

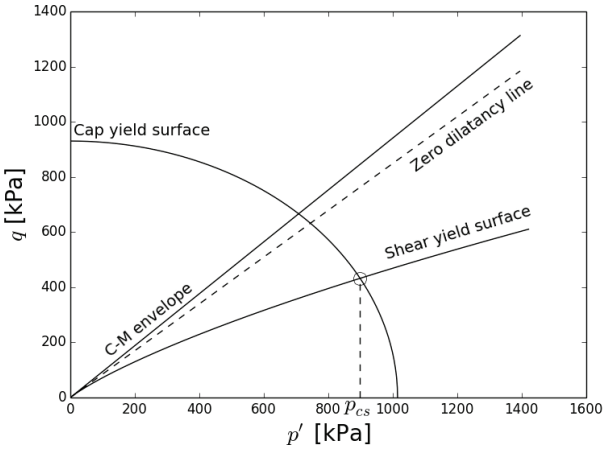

Fig. 2. Graphical representation of p_{cs} value

$$\begin{aligned} f_1(\widetilde{\sigma}_{ij}, \gamma^{PS}) &= 0, \\ f_2(\widetilde{\sigma}_{ij}, p_c) &= 0, \end{aligned} \qquad (14)$$

in which $f_1(\widetilde{\sigma}_{ij}, \gamma^{PS})$ represents the current shear yield condition while $f_2(\widetilde{\sigma}_{ij}, p_c) = 0$ the volumetric (cap) one. It can easily be proved that the sought stress state $\widetilde{\sigma}_{ij}$ preserves same Lode angle as the current one σ_{ij}.

4. UNDRAINED TRIAXIAL TEST ON NORMALLY CONSOLIDATED AND OVERCONSOLIDATED SAMPLES

In order to demonstrate how the modified model can reproduce the ultimate deviatoric stress in the undrained triaxial compression conditions, four single element tests were run assuming OCR = 1, 4, 10, 40. The initial effective pressures were equal to p' = 1000 kPa, p' = 250 kPa, p' = 100 kPa and p' = 25 kPa, respectively. The standard HS model was used for all the tests. The assumed set of model parameters used in the test was as follows: σ_{ref} = 100 kPa, ν_{ur} = 0.2, m = 0.5, $E_{\mathrm{ur}}^{\mathrm{ref}}$ = 50000 kPa, E_{50}^{ref} = 12000 kPa, ϕ = 24°, ψ = 2°, c = 0 kPa, R_f = 0.9, D = 0.0, f_t = 0 kPa, H = 12745.75 kPa, M = 0.9215. To visualize differences between models with uncoupled and coupled hardening four additional predictions were made using classical HS model with OCR = 1, 4 and ψ = 0°/2°.

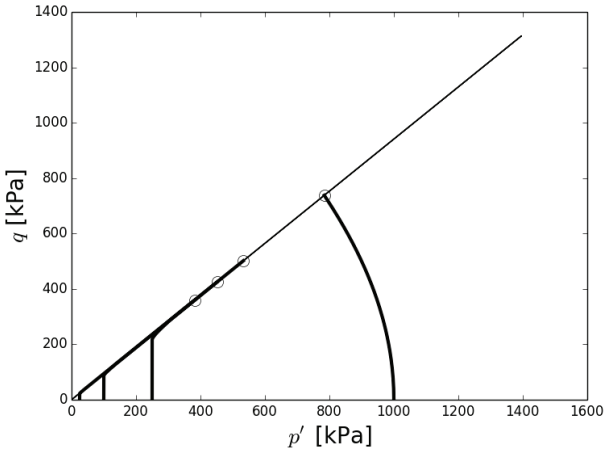

Fig. 3. Effective stress paths for different values of OCR (OCR = 1, 4, 10, 40)

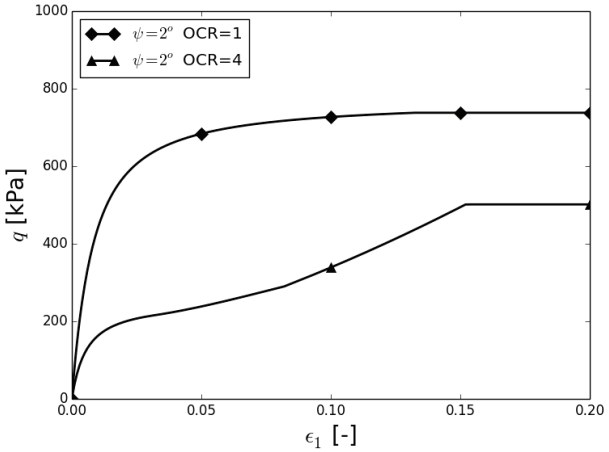

Fig. 4. Shear characteristics $q - \varepsilon_1$ resulting from the coupled model, obtained for OCR = 1, 4 and $\psi = 2°$

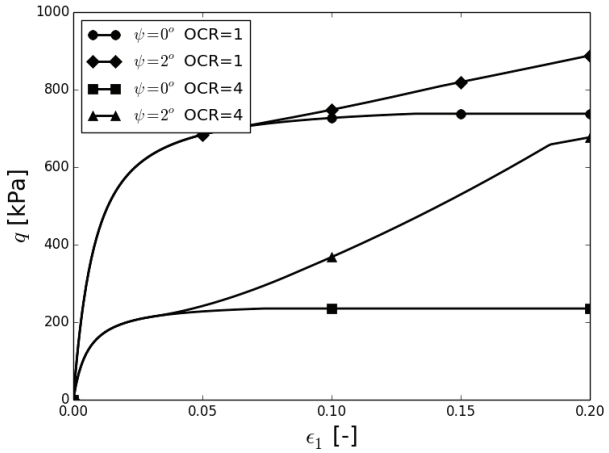

Fig. 5. Shear characteristics $q - \varepsilon_1$ resulting from the uncoupled model, obtained for OCR = 1, 4 and $\psi = 0°/2°$

The resulting effective stress paths for the model with coupled plastic mechanisms are shown in Fig. 3. It is well visible that the ultimate deviatoric stresses (shown in the figure as circular markers) are decreasing with the increasing OCR value. The corresponding $q - \varepsilon_1$ curves for the model with coupling and two selected values of OCR = 1, 4 are shown in Fig. 4. We can notice that the ultimate deviatoric stress tends to the asymptotic value. This effect is not observed for the standard HS model (without coupling) once the dilatancy angle $\psi > 0$ (see Fig. 5).

5. TUNNEL IN LONDON CLAY CASE STUDY

The following case study demonstrates an application of the HSs model to simulate a tunnel construction boundary value problem. The use of HSs model allows pre-failure nonlinearities and strongly non-linear stiffness variation to be accounted for. This study revisits the excavation model of the twin Jubilee Line Extension Project tunnels beneath St James's Park (London, UK) which was reported in the original paper by Addenbrooke et al. [2]. In this study, we focus on comparing uncoupled and coupled dilatancy models with the measured field data.

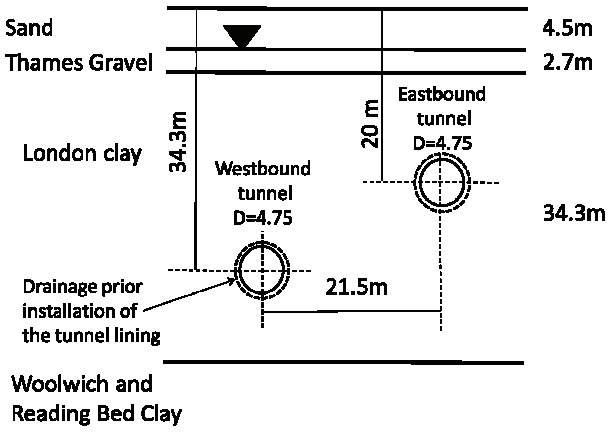

Fig. 6. Soil stratigraphy and diagonally oriented tunnels at St James's Park, London, UK

Table 1. Material parameters of London clay for HSs model
(stiffness parameters are set at the reference stress $\sigma_{ref} = 360$ kPa)

E_0^{ref}	$\gamma_{0.7}$	E_{ur}^{ref}	ν	E_{50}^{ref}	m	ϕ	ψ	c	γ_D	e_0
[kPa]	[–]	[kPa]	[–]	[kPa]	[–]	[°]	[°]	[kPa]	[kN/m^3]	[–]
$390 \cdot 10^3$	$3 \cdot 10^{-4}$	$75 \cdot 10^3$	0.2	$35 \cdot 10^3$	0.75	25.0	12.5	5.0	16.2	0.6

The problem statement, i.e., subsurface stratigraphy and the orientation of tunnels is presented in Fig. 6. In keeping with the original paper, only the London clay layer was modeled with the aid of the advanced constitutive law whereas all other layers are represented by the Mohr–Coulomb model and the most upper one is simply elastic. Stiffness parameters of the HSs model, i.e., E_0^{ref}, E_{ur}^{ref}, E_{50}^{ref} were calibrated based on isotropically consolidated undrained extension triaxial test. Their values are summarized in Table 1. The exponent m was assumed equal to 0.75 as reported by Viggiani et al. [14]. A similar value of E_0^{ref} to the calibrated E_0^{ref} = 390 000 kPa has also been reported by Gasparre [5]. Strength and plastic potential parameters – values typical of London clay have been adapted from the original paper for all the models considered. The value of the overconsolidation ratio OCR for London clay was assumed equal to 15 as it is typically observed for depths around 20–30 meters. Due to heavy over-consolidation, K_0 coefficient, in the London clay, was assumed equal to 1.0 in the analysis. The sand layer was modeled as an elastic material characterized by E = 5000 kPa, ν = 0.2, γ_D = 18 kN/m^3, e_0 = 0.25 K_0 = 0.5. The gravel layer was modeled as an elastic ideal plastic material characterized by stiffness modulus varying with depth starting from E = 27000 kPa to E = 35 000 kPa, ν = 0.2, ϕ = 35°, ψ = 17.5°, c = 0 kPa, γ_D = 18 [kN/m^3], e_0 = 0.25, K_0 = 0.5. The Woolwich Bed Clay was also modeled as the Mohr–Coulomb material characterized by stiffness modulus varying with depth starting from E = 156 000 kPa to E = 234000 kPa, ν = 0.2, ϕ = 27°, ψ = 13.5°, c = 200 kPa, γ_D = 16 kN/m^3, e_0 = 0.6, K_0 = 1.0.

As far as seepage properties are concerned, sand and gravel layers were modeled as highly permeable materials ($k = 10^{-5}$ m/s was assumed for sands and $k = 10^{-4}$ m/s for gravels) with S_r = 0.0 and α = 2.0, whereas clayey soils were attributed with an anisotropic permeability decreasing with depth, i.e., $k_v = 10^{-9} \div 10^{-10}$ m/s and $k_h = 10^{-8} \div 10^{-10}$ m/s (S_r = 0.1, α = 0.001). Characteristics for the tunnel lining which were adopted after the original paper are summarized in Table 2.

Table 2. Tunnel lining parameters

Young's modulus E	Poisson's ratio ν	Cross sectional area A	Momentum of inertia I_z	Lining-soil interface friction angle
[GPa]	[–]	[m^2/m]	[m^4/m]	[°]
28	0.15	0.168	3.95136	20

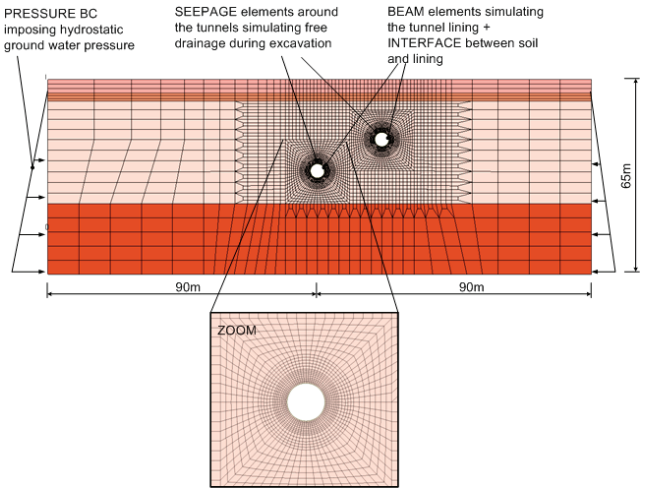

Fig. 7. Finite element mesh

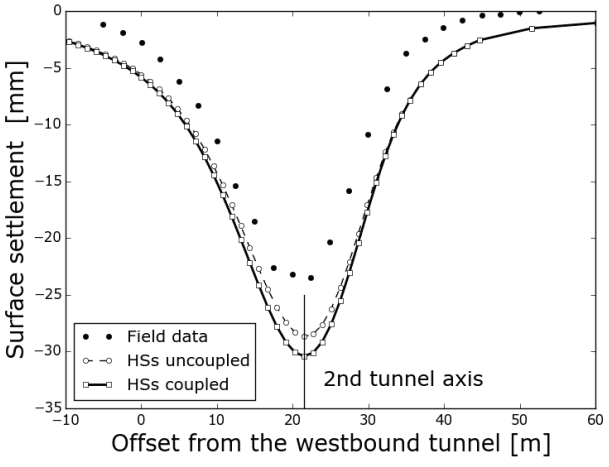

Fig. 8. Surface settlements above the eastbound tunnel after its excavation: field data vs. comparison of uncoupled and coupled models

The finite element discretization of the plane-strain consolidation model, generated within the ZSoil program, is shown in Fig. 7. A relatively dense mesh is used

near the tunnels and a coarse one elsewhere. The two versions of the HSs model are used, i.e., with and without coupling shear and volumetric plastic mechanisms, respectively. The computed distribution of surface settlements above the eastbound tunnel (secondarily excavated one), after its excavation, compared with the field measurements is shown in Fig. 8. As expected, the coupled HSs model yields slightly larger settlements with respect to the uncoupled version. The difference is not significant in the case considered since the undrained shear limit occurs mainly in a narrow zone in the close vicinity of the tunnel walls and the amplitude of the deviatoric strain is not large. The obtained prediction is relatively good and major discrepancies are observed at larger distances from the eastbound tunnel axis. This may likely result from the application of the elastic and ideally elastic-perfectly plastic models for upper soil layers (sands and gravels). In order to illustrate the differences between the two analyzed versions of HS model, the effective stress paths measured at wall arch at 45° in the westbound tunnel are plotted (see Fig. 9). As could be expected, larger values of the unlimited deviatoric stress are generated by the uncoupled model, whereas the modified model reduces an artificial strength gain.

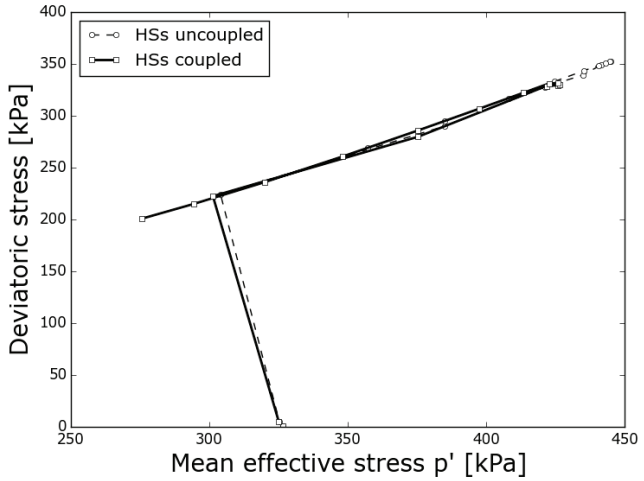

Fig. 9. Effective stress paths occurred in the element adjacent to the tunnel wall arch at 45° in the westbound tunnel

Clearly, small strain stiffness is one of the most important factors affecting prediction of deformations occurring around the tunnel. However, the surface settlement relief is a resultant not only of the pre-failure, but also of the ultimate undrained soil behavior appearing in the vicinity of the excavated tunnel. In practice, an improper modeling of the undrained shear strength of cohesive soils (original formulation of the HS model) may lead to overestimation of soil resistance. This drawback may yield insecure solutions (underestimated subsoil deformations and sectional forces in structural members) in certain class of soil-structure interaction problems.

6. CONCLUSIONS

The efficient remedy to the major drawback of the original Hardening Soil model which exhibits inability to appropriately predict the undrained shear strength was proposed and verified on single element test problems. The modified model was validated on the 2D boundary value problem of the twin-tunnel excavation in London clay. In order to integrate an upper limit to the undrained shear strength to the model, the evolution law for the p_c state parameter was expressed as a function of the sum of volumetric plastic strain increments resulting from the two plastic mechanisms, i.e., shear and the volumetric one, respectively. This coupling was enhanced by an additional modification of Rowe's dilatancy law in the dilatant domain, in which value of sin function of the mobilized dilatancy angle $\sin\psi_m$ is weighted by a smooth function varying from zero to one depending on the relation between the current mean effective stress p with respect to the pressure corresponding to the intercept of the current shear and cap yield surfaces p_{cs}. The proposed modification preserves continuity of the function $\sin\psi_m$. Moreover, it can easily be proved that softening behavior is precluded. The latter fact is of primary importance in complex engineering computations carried out with the aid of implicit finite element codes. A more detailed analysis of the proposed formulation in the context of the SHANSEP concept and some selected algorithmic issues related to the proposed model modifications will be discussed in the further authors' paper.

REFERENCES

[1] *ZSoil manual*, Elmepress and Zace Services Limited, Lausanne, Switzerland, 2014.

[2] ADDENBROOKE T., POTTS D., PUZRIN A., *The influence of pre-failure soil stiffness on the numerical analysis of the tunnel construction*, Geotechnique, 1997, 47(3), 693–712.

[3] AUBRY D., OZANAM O., *Free-surface tracking through non-saturated models*, [in:] Swoboda (ed.), *Numerical Methods in Geomechanics*, Balkema, Innsbruck, 1988, 757–763.

[4] BENZ T., *Small-strain stiffness of soils and its numerical consequences*, Ph.D. thesis, University of Stuttgart, 2006.

[5] GASPARRE A., *Advanced laboratory characterisation of London clay*, Ph.D. thesis, Imperial College, 2005.

[6] IRMAY S., *On the hydraulic conductivity of unsaturated soils*, Trans. Am. Geophys. Union, 1956, 35, 463–468.

[7] LADD C., FOOTT R., *New design procedure for stability of soft clays*, Journal of the Geotechnical Engineering Division ASCE, 1974, 100 (7), 763–786.

[8] OBRZUD R., TRUTY A., *The hardening soil model – a practical guidebook*, Technical Report Z Soil, PC 100701, Zace Services, Ltd., 2013.

[9] SCHANZ T., *Zur Modellierung des mechanischen Verhaltens von Reinbungsmaterialien*, Mitt. Inst., für Geotechnik, 45, Universitat Stuttgart, 1998.

[10] SCHANZ T., VERMEER P., BONIER P., *Formulation and verification of the Hardening Soil Model*, Beyond 2000 in Computational Geotechnics, Balkema, Rotterdam, 1999.

[11] TRUTY A., *On certain classes of mixed and stabilized mixed finite element formulations for single and two-phase geomaterials*, Zeszyty Naukowe Politechniki Krakowskiej, Seria Inżynieria Środowiska 48, Kraków, 2000.

[12] TRUTY A., ZIMMERMANN T., *Stabilized mixed finite element formulations for materially nonlinear partially saturated two-phase media*, Computer Methods in Applied Mechanics and Engineering, 2006, 195, 1517–1546.

[13] VAN GENUCHTEN M.T., *A closed form equation for predicting the hydraulic conductivity of unsaturated soils*, Soil Sciences Am. Soc., 1980, 44, 892–898.

[14] VIGGIANI G., ATKINSON J., *Stiffness of fine grained soil at very small strain*, Geotechnique, 1995, 45(2), 249–265.